Journal of Catalysis **202,** 68–77 (2001)
doi:10.1006/jcat.2001.3280, available online at http://www.idealibrary.com on IDEAL®

Comparative Vapor Phase Synthesis of ETBE from Ethanol and Isobutene over Different Acid Zeolites

F. Collignon[1] and G. Poncelet[2]

Université Catholique de Louvain, Unité de Catalyse et Chimie des Matériaux Divisés, Place Croix du Sud 2/17, B-1348 Louvain-la-Neuve, Belgium

Received November 13, 2000; revised May 14, 2001; accepted May 20, 2001

Vapor phase synthesis of ETBE from ethanol and isobutene has been investigated over US-Y, Beta, and ZSM-5 zeolites with different Si/Al ratios, using Amberlyst-15 as a reference catalyst. The zeolites were characterized by X-ray diffraction and nitrogen adsorption–desorption isotherms at 77 K. Total acidity of the Beta zeolites was determined by ammonia-TPD measurements whereas IR spectroscopy was used to investigate the OH stretching region and evaluate the Brønsted and Lewis acid contents by pyridine adsorption. Beta zeolites, with higher external surface area, were more active than the other zeolites. The highest yields of ETBE were obtained for Beta samples with high Brønsted acid content and low SiOH/AlOHSi ratio. © 2001 Academic Press

Key Words: **ETBE; vapor phase synthesis; zeolites; H-Beta; US-Y; H-ZSM-5; external surface area; Brønsted acidity; silanol groups.**

INTRODUCTION

Methyl tertiary-butyl ether (MTBE) and ethyl tertiary-butyl ether (ETBE) are octane enhancers of unleaded gasolines. Both ethers easily mix with gasoline (10–15 vol.%), have excellent antiknocking behavior, and reduce emission of carbon monoxide and unburned hydrocarbons (1). MTBE production largely overwhelms that of ETBE because of the greater availability and lower production cost of methanol relative to ethanol (2). ETBE has the advantage over MTBE of a lower vapor pressure, and ethanol is a renewable energy source (bio-ethanol). Recently, a novel ether, the 3-methoxy-3-methylpentane, obtained by the etherification of 2-ethyl-1-hexene with methanol, has been proposed as a possible candidate (3).

The synthesis of these oxygenates is commercially operated in liquid phase over sulfonic acid resins, at temperatures in the 50–70°C range, pressures between 10 and 15 bar, and alcohol/isobutene molar ratios in excess of stoichiometry (4). Sulfonic acid resins are relatively inexpensive and well-performing catalysts. Because ether synthesis is exothermic, temperature needs to be carefully controlled to avoid the release of temperature-sensitive sulfonic groups from the matrix, which causes a loss of activity and corrosion problems (5). Since the process is operated with alcohol/isobutene molar ratios is excess of stoichiometry, recycling is necessary. The kinetics and mechanism of ETBE formation in liquid phase conditions have been investigated by several authors. Françoisse and Thyrion (6) observed that ethanol was preferentially adsorbed inside the porosity of Amberlyst-15 due to its polarity, and they proposed Eley–Rideal and Langmuir–Hinshelwood reaction mechanisms depending on ethanol concentration. Heat capacity and reaction enthalpy measurements obtained by Sola *et al.* (7) with reaction calorimetry techniques confirmed the E–R model established from kinetic studies (8). Cunill *et al.* (9) observed that the production rates of ETBE and MTBE were strongly lowered by small amounts of water, particularly at the beginning of the reaction. This inhibitor effect disappeared with progressive formation of *tert*-butyl alcohol.

The synthesis of ETBE over nonresin catalysts is much less documented relative to MTBE. Acid zeolites are stable in the temperature domain where the ethers are formed. They could be attractive catalysts provided that their efficiency at the low temperatures imposed by the thermodynamics of the reaction (10) is high enough. Results of Tau and Davis (11) showed that the isobutene to ETBE conversion over H-ZSM-5 was relatively low compared with Amberlyst-15. The protective effect of ethanol clusters on the acid sites of H-mordenite would be responsible for the inhibiting effect of ethanol; it would also prevent isobutene oligomerization and ensure the zeolite stability (12). A reaction pathway involving the attack of the C=C bond of isobutene by a single hydrogen-bonded ethanol molecule was proposed. Vapor phase synthesis of ETBE over gallophosphate cloverite gave a maximum yield of ETBE of 20% at 102°C and a selectivity of 83–84% (13, 14).

A previous study on the vapor phase synthesis of MTBE over different zeolites showed that H-Beta was as active as Amberlyst-15 and superior to US-Y, H-mordenites,

[1] Present address: Katholieke Universiteit Leuven, Centrum voor Oppervlaktechemie en Katalyse, Kasteelpark Arenberg 23, B-3001 Leuven, Belgium.

[2] To whom correspondence should be addressed. E-mail: poncelet@cata.ucl.ac.be.

0021-9517/01 $35.00

H-ZSM-5, and other zeolites (15), a result confirmed both in vapor (16–19) and in liquid phase conditions (20).

This study reports on comparative screening experiments of the vapor phase synthesis of ETBE over different zeolites and Amberlyst-15. Emphasis has been given to H-Beta zeolites because of their higher catalytic performances. In particular, their activation mode and the role of the acid and silanol contents have been addressed.

EXPERIMENTAL

Catalysts

The different zeolites considered in this study are listed in Table 1. The US-Y zeolites (series CBV 500 to CBV 780), Beta zeolites (B75, B25, B25*, with the asterisk indicating a different batch, and B25t, with t standing for a sample still containing its template tetraethyl ammonium), and ZSM-5 (CBV3020 to CBV8020, and CBV2802, a silicalite-type) were commercial samples kindly supplied by PQ Zeolite. Sample B25 is the same batch used in previous studies (15, 20). Bsc was a Beta zeolite provided by Süd-Chemie. Mordenite was a large-port variety (HSZ640 from Tosho Corp., Japan) that was steam-dealuminated at 600°C and acid leached to remove extra framework Al species (21). This sample was among the most active mordenites in a previous study (15). LZ-6 (Omega zeolite) was a sample from Union Carbide. The series of US-Y, Beta, and H-ZSM-5 were used as received, except for three samples in the ammonium form (CBV500, CBV 712, and CBV8020), which were previously decationated under the conditions indicated below.

Samples of B25* were dealuminated using a method similar to that of Fajula *et al*. (22). Zeolite (1 g) was added to 200 ml of HNO_3 solution previously heated at 80°C, and the mixture was stirred for 3 h at this temperature. Acid concentrations were in the range 0.02–0.09 M (samples B25*0.02 to B25*0.09 in Table 1). The solids were washed and dried at 100°C for 1 h.

Beta zeolites with Si/Al ratios of 9.2, 14.6, and 17.9 (samples lB-t for lab-synthesized Beta in Table 1) were synthesized in the presence of tetraethyl ammonium hydroxide (TEAOH) as a template, following a reported procedure (23). Briefly, TEAOH (35 wt% aqueous solution, Aldrich) was mixed in deionised water with sodium aluminate (37 wt% Na_2O, 56 wt% Al_2O_3, Carlo Erba) in a teflon cylinder and stirred for 10 min. Silica (FK300DS, Degussa) was progressively added to the solution. The SiO_2/TEAOH and H_2O/SiO_2 molar ratios were 6 and 6.1, respectively. The Si/Al molar ratio of the "dry" mixture was changed by adjusting the amount of sodium aluminate. The powder was mixed at 60–70 rpm for 30–40 min until a thick slurry was obtained. Crystallization was carried out in a nonstirred Parr pressure vessel (using Teflon containers) heated for 48 h at 170°C. The solid was washed by filtration with hot demineralized water (25 ml per g of solid) and dried at 60°C.

TABLE 1

Si/Al Ratio, Relative Crystallinity (%), External Surface Area (S_{ext}, $m^2\ g^{-1}$), Micropore Volume (V_μ, $cm^3\ g^{-1}$), Al Content (mmol g^{-1}), NH_3-TPD (mmol g^{-1}), and Enthalpy of Ammonia Desorption (ΔH, kJ mol^{-1})

	Si/Al	Rel. Cryst.	S_{ext}	V_μ	Altot.[a]	NH_3-TPD	ΔH^b
Zeolite Beta							
Bsc	24.6	97	182	0.18	0.65	0.45	123
B75	36.0	96	261	0.18	0.45	0.41	123
B25	12.2	100	282	0.19	1.26	0.89	121
B25*	13.4	98	241	0.16	1.16	0.46	119
B25* 0.02	17.4	92	n.d.[c]	n.d.[c]	0.89	0.55	119
B25* 0.03	19.1	92	255	0.18	0.87	0.52	119
B25* 0.05	22.0	89	252	0.16	0.74	0.54	121
B25* 0.06	23.6	96	n.d.	n.d.	0.73	0.50	120
B25* 0.09	31.4	89	263	0.18	0.56	0.42	120
lB18t c	9.2	88	188	0.19	1.63	1.12	122
lB18t cec	9.2	83	179	0.13	1.63	1.43	117
lB28t c	14.6	100	278	0.21	1.07	0.95	123
lB28t cec	14.6	82	263	0.18	1.07	1.02	122
lB36t c	17.9	93	167	0.16	0.88	0.81	121
lB36t cec	17.9	93	225	0.13	0.88	0.77	120
B25t c	11.8	93	233	0.19	1.30	1.05	119
B25t cec	11.8	78	n.d.	n.d.	1.30	1.02	118
B25t 0.1 c	14.0	92	n.d.	n.d.	1.11	1.24	118
US-Y							
CBV500	2.6	100	85	0.26	4.63	1.51	116
CBV600	2.8	91	96	0.22	4.38	0.83	115
CBV712	5.8	121	116	0.25	2.47	0.69	118
CBV760	30.0	40	119	0.26	0.54	0.27	127
CBV780	37.0	89	136	0.26	0.44	0.17	127
ZSM-5							
CBV3020	16.5	79	63	0.16	0.95	0.93	128
CBV5020	25.0	85	35	0.18	0.64	0.62	130
CBV8020	38.3	81	56	0.17	0.42	0.47	129
CBV2802	137.5	100	n.d.	n.d.	0.12	n.d.	n.d.
Mordenite							
M-S600H6	117.4	93	87	0.19	0.14	0.13	n.d.
Omega							
LZ-6	4.5	100	n.d.	n.d.	3.03	n.d.	n.d.

[a] From ICPS;
[b] Calculated according to (26, 27).
[c] n.d.: not determined.

Samples were either calcined to eliminate the template (lBt c), or calcined, subsequently ammonium-exchanged, and calcined again to obtain the protonic forms (lBt cec).

Elimination of the template from B25t and the lab-synthesized Beta zeolites (lB-t) was achieved in leached-bed conditions by temperature-programmed calcination between room temperature and 120°C, with a plateau for 1 h, and from 120 to 540°C in flowing nitrogen (250 ml min^{-1}) with a ramp of 5°C min^{-1}. At 540°C, nitrogen was switched with oxygen, and the treatment was maintained for an additional 2.5 h (samples marked "t c" in tables).

A few Beta zeolites (cec in Table 1) were calcined to remove the template and then converted to the NH_4^+-form

by adding 1 g zeolite to 200 ml of a 2 M ammonium acetate solution heated at 80°C and stirred overnight. After filtration, washing, and drying at 60°C for 1 h, the samples were calcined to obtain the H^+-form. Calcination was done under flowing air using the same ramp as above, except that the final temperature (500°C) was maintained for 10–15 h. The ammonia evolved during the whole treatment was collected and quantified as for the NH_3-TPD measurements.

Amberlyst-15 (a sulfonic acid resin from Aldrich), with surface area of 50 m^2 g^{-1} and cation exchange capacity of 4.9 mequiv. g^{-1}, was used as a reference catalyst. It was previously washed following a procedure reported in the literature (24).

Characterization

The relative crystallinity of the dealuminated samples was evaluated from the X-ray diffraction patterns recorded with a Siemens D-5000 apparatus (with monochromatized Cu-Kα radiation) relating, for the Beta zeolites, the area of the [302] reflection (at 22.43° 2θ) to that of sample B25. For the ZSM-5 and the US-Y zeolites, the sum of the areas of the main reflections was reported to that of samples CBV2802 and CBV500, respectively. The bulk Si/Al ratios were established from the Al contents (Altot in Table 1) obtained by inductively coupled plasma spectroscopy. The textural properties were obtained from nitrogen adsorption–desorption isotherms recorded at 77 K with an ASAP 2000 sorptometer (Micromeritics), using the *t*-plot method for the determination of the external surface areas (S_{ext}) and micropore volumes (V_μ) (for *t* values in the range 0.35–0.5 nm) (25).

Temperature-programmed desorption of ammonia (NH_3-TPD) was carried out adopting the experimental conditions of Niwa *et al.* (26) and Katada *et al.* (27). The release of ammonia in the gaseous effluent was followed with a thermal conductivity detector, with the ammonia being continuously collected at the outlet of the TCD in a 0.2 M solution of H_3BO_3. Back titration with 0.005 M H_2SO_4 provided the total amount of ammonia evolved from the zeolite.

FTIR spectroscopy was used to examine the OH stretching region of the Beta zeolites before and after adsorption of pyridine. Self-supporting wafers (1.54 cm^2) obtained by compression were outgassed in the IR cell at 400°C for 2 h (10^{-5} torr). After cooling at room temperature and recording the spectrum, pyridine was admitted in the cell and equilibrated for 15 min. The cell was then outgassed under vacuum at increasing temperatures, with intermediate spectra being recorded after cooling at ambience. The areas of the different bands were normalized to the weight of the wafers (10–30 mg). It was verified that the integrated area of the Si–O band at 1870 cm^{-1} was proportional to the weight of the wafer.

Catalytic Measurements

The reaction was carried out in vapor phase in a fixed bed U-shaped glass microreactor operated at atmospheric pressure, with ethanol/isobutene (EtOH/IB) molar ratio of 1 and WHSV of 2 h^{-1}. Ethanol vapor was generated by flowing a stream of helium (7.9×10^{-4} mol min^{-1}) through a glass saturator thermostated at 28°C. The flows were monitored with mass-flow controllers. The reaction was studied in the temperature range 36–100°C at a heating rate of 0.3°C min^{-1}, with a thermocouple placed near the catalyst bed allowing continuous control of temperature. Tubings, valves, and connections in front of the reactor were heated at 60°C, and those between the reactor outlet and the gas chromatograph were heated to 120°C. Prior to the catalytic evaluation, activation of the zeolites (typically 200 mg) was done in situ at 400°C for 3 h in flowing helium. The acid resin was treated in situ at 90°C for 3 h in flowing helium. Online gas phase analysis was done in a gas chromatograph (5890 from Hewlett-Packard) equipped with TC detector and 30-m capillary column (cross-linked methyl silicone from Hewlett-Packard). Sampling of the gaseous effluent was monitored every 16.67 min by means of an automated six-way sampling valve. The conversions, yields, and selectivities were calculated from the number of moles of reacted and nonreacted isobutene.

RESULTS

Characterization

The bulk Si/Al ratios, relative crystallinities, and textural characteristics (S_{ext} and V_μ) of the different zeolites are compiled in Table 1. Except for CBV760, the relative crystallinities were satisfactory with, for all the Beta zeolites, values above 80%.

As expected, the US-Y zeolites had greater micropore volumes than the H-Beta zeolites and H-mordenite, with the lowest values for the H-ZSM-5 zeolites. Dealuminated US-Y zeolites exhibited increased external surface area. All the Beta zeolites had higher external surface areas than the other zeolites, owing to their very small crystallite size (20 nm) (28).

The acid contents obtained from the ammonia-TPD measurements, the total Al content (Altot, in mmol g^{-1}), and the desorption enthalpies providing an estimation of the average strength of the acid sites calculated according to Refs. (26, 27) are given in Table 1. ZMS-5 and the most dealuminated US-Y samples exhibited slightly higher desorption enthalpies.

Several commercial samples and the lab-synthesized Beta zeolites had NH_3-TPD values close to the total Al content, suggesting that each Al generated an acid site. B25 had more accessible acid sites (NH_3-TPD) than B25*, in spite of a same origin and similar Si/Al ratio (probably different syntheses). Leaching B25* with 0.02 to 0.09 M HNO_3

TABLE 2

Normalized Surface Area of Different OH Bands (u.a. g^{-1}), and Relative Amounts of Brønsted and Lewis Acidities (in mmol $\cdot g^{-1}$) after Pyridine Adsorption and Outgasing at 150°C

	VHF ~3780 cm^{-1}	SiOH 3738–3745 cm^{-1}	AlOH ~3660 cm^{-1}	AlOHSi 3607–3615 cm^{-1}	Pyridine-Brønsted 1545 cm^{-1}[a]	Pyridine-Lewis 1454 cm^{-1}[a]
Bsc	n.b.[b]	1132	n.b.	144	0.29	0.22
B75	n.b.	1466	n.b.	141	0.18	0.07
B25	2	1045	6	199	0.34	0.28
B25*	13	1552	47	46	0.29	0.28
B25* 0.03	28	1181	2	57	0.39	0.30
B25* 0.05	31	1807	1	97	0.25	0.17
B25* 0.06	33	1830	n.b.	112	0.33	0.19
B25* 0.09	8	1133[c]	n.b.	79	0.33	0.19
lB18t c	7	813[c]	0.2	607	0.52	0.23
lB18t cec	n.b.	953[c]	n.b.	801	0.63	0.27
lB28t cec	n.b.	1046[c]	n.b.	440	0.28	0.15
lB36t cec	n.b.	756[c]	n.b.	267	0.21	0.08
B25t c	7	1350[c]	n.b.	690	0.58	0.37

[a] Calculated with $\varepsilon_B = 1.67$ cm μmol^{-1} and $\varepsilon_L = 2.22$ cm μmol^{-1} (42).
[b] n.b.: no band.
[c] Majority of SiOH groups in external position ($\nu \geq 3743$ cm^{-1}).

increased the Si/Al ratio from 12.5 to 31.4. For these samples, the normalized area of the band near 3610 cm^{-1} (bridging AlOHSi groups) increased with increasing acid concentrations (except for the sample treated with 0.09 M HNO_3) (Table 2), indicating that extra-framework Al (EFAL) species neutralizing acid sites or blocking their access (28) were removed by a mild acid leaching. Sample B75 had very few EFAL as inferred from the NH_3-TPD/Altot molar ratio close to 1 (Table 1) and the low content of Lewis acid sites (Table 2).

B25t c (supplied with its template and calcined) exhibited a greater amount of acid sites compared with B25 and B25* (both with similar Al contents). Interestingly, B25t 0.1-c (treated with 0.1 M HNO_3 and calcined to remove the template) desorbed the highest amount of ammonia among the Beta zeolites. The samples with Si/Al ratio higher than 11 (B25t, lB28t, and lB36t) calcined without (-c) and with an intermediate ammonium exchange (-cec) had similar acid contents, thus indicating that an intermediate ammonium exchange is not indispensable.

The US-Y zeolites exhibited large differences between the Altot and the NH_3-TPD values, particularly CBV500, CBV600, and CBV712. ^{27}Al MAS-NMR spectra of those zeolites showed signals at 0 and 30 ppm typical of EFAL species (29). CBV760 and CBV780 had very few EFAL species. The number of acid sites measured by TPD agreed well with the tetrahedral Al determined by ^{27}Al MAS-NMR (1.64, 0.88, 0.75, 0.22, and 0.13 mmol g^{-1}, for CBV500, CBV600, CBV712, CBV760, and CBV780, respectively) (15, 29). This correspondence supports the validity of the procedure adopted for the quantification of the accessible acid sites.

The ZSM-5 zeolites had similar Altot and NH_3-TPD values, thus ruling out significant amounts of EFAL species. They also had acid sites with higher average strength compared with the other zeolites, as inferred from the higher desorption enthalpies.

Typical IR spectra of commercial (B25*) and lab-synthesized Beta zeolites (lB36t cec) are shown in Fig. 1. Five bands appeared in the OH stretching region. The two intense bands at 3745 and 3738 cm^{-1} are characteristic of silanol groups at external and internal (hydroxyl nest) positions, respectively (30–36). The high relative intensity of these bands in Beta zeolite has been accounted for by the small crystallite size and the existence of structural defects (coexistence of three unit cells) (37, 38). The

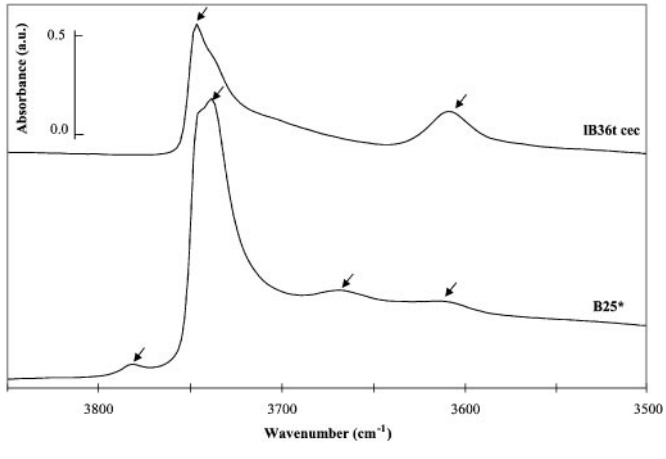

FIG. 1. IR spectra in the O–H stretching region of B25* (commercial) and lB36t cec (lab-synthesized) Beta zeolites.

integrated areas of the different OH bands normalized to the sample weights are given in Table 2. Compared with the commercial samples, the lab-synthesized zeolites (samples lBt) had fewer SiOH groups, with a higher proportion at external than internal position, and also more bridging AlOHSi groups (band at 3610 cm^{-1}), consistently with the higher NH_3-TPD values (Table 1). The bands at 3660 and 3780 cm^{-1} were mainly observed over the commercial samples. According to Jia *et al.* (33), the intensity of these bands increases when hot spots or self-steaming conditions are favored during the calcination (deep-bed conditions and/or temperature higher than 500°C). The band at 3780 cm^{-1} has recently been attributed to a hydroxyl group on a tri-coordinated Al partially connected to the framework (39). These OH groups have a weaker acid character than those absorbing at 3610 and 3660 cm^{-1} (31, 40). The band at 3660 cm^{-1} has been assigned to extra-framework AlOH groups (32, 34) or OH groups bonded to tetrahedral Al partially disconnected from the framework (41).

The acidity of the Beta zeolites was also investigated by IR spectroscopy of adsorbed pyridine. After adsorption of pyridine and subsequent outgassing, the bands at 3780 (VHF), 3660, and 3610 cm^{-1} disappeared, thus verifying their acidic character. The relative quantities of the Brønsted and Lewis acid sites estimated from the normalized areas of the bands at 1545 (Py-B) and 1446 cm^{-1} (Py-L) (samples outgassed at 150°C) corrected by the respective extinction coefficients of Emeis (42) are given in Table 2. The relation between the integrated areas of the Py-B band at 1545 cm^{-1} versus the bridging OH at 3610 cm^{-1}, both normalized to the sample weight, is shown in Fig. 2a. A similar relationship was observed between the NH_3-TPD values and the integrated area of that same band (figure not shown here). The fact that the relationship did not pass through the origin is probably related to the presence of reversible Al, typical of Beta zeolites (30), and/or to different AlOH Brønsted acid sites (bands at 3780 and 3660 cm^{-1}). A relation was also observed when plotting the normalized areas of the Py-L band at 1445 cm^{-1} against the difference between the total Al content (Al_{tot}) and the NH_3-TPD values (Fig. 2b). Except for the EFAl-rich B25* and the nonexchanged lB18t c samples, the Lewis acid content increased with the EFAL content.

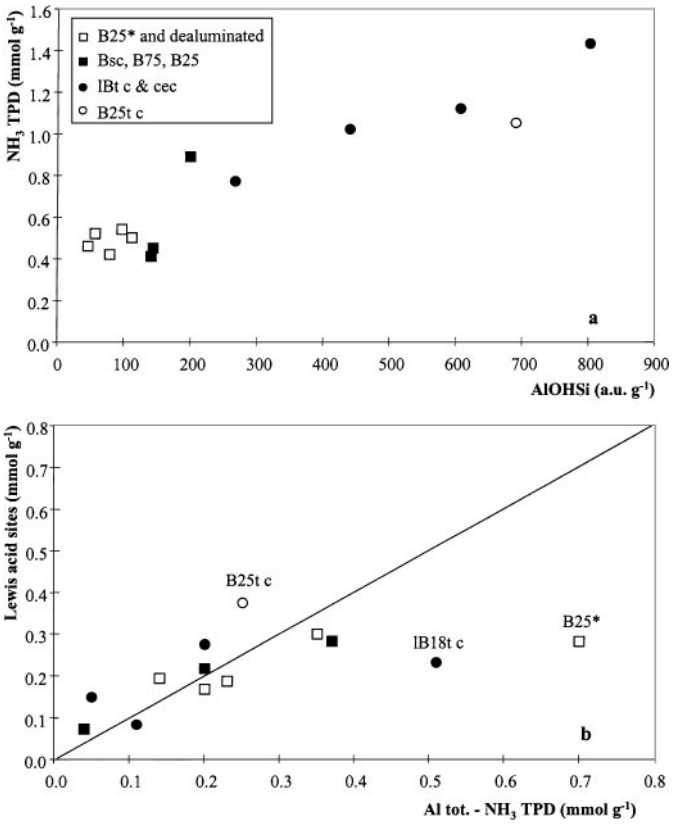

FIG. 2. (a) Relation between total acidity determined by NH_3-TPD (mmol g^{-1}) and normalized band area of the bridging AlOHSi groups (in a.u. g^{-1}). (b) Relation between Lewis acidity determined by pyridine (normalized area of the band at 1456 cm^{-1}, a.u. g^{-1}) and the difference between total Al and acid content determined by NH_3-TPD (mmol g^{-1}).

Catalysis

The yield of ETBE versus reaction temperature curves all exhibited a similar shape. With increasing temperature, the IB to ETBE conversion increased, reached a maximum, and decreased beyond this maximum, with the most active catalysts operating the synthesis at lower temperatures. The decreasing part of the curves superimpose, as imposed by the thermodynamic equilibrium of the reaction at each temperature. The yields of ETBE at 45°C and at maximum IB to ETBE conversion, and the yields of C8 at 100°C obtained over the different series of zeolites, are compiled in Table 3. CBV760 and CBV712 were more active than the other US-Y zeolites, with a maximum ETBE yield of 10–11% at about 80°C. CBV760 also was the most active one in the vapor phase synthesis of MTBE (15). None of the US-Y zeolites was active at 45°C. The ZSM-5 zeolites were all less efficient than the US-Y ones, with yields at maximum conversion barely exceeding 5% (at around 90°C), namely, half the value obtained over the best US-Y zeolites, and with only a limited effect of the Si/Al ratio (between 16.5 and 38.3). ZSM-5 with Si/Al = 137.5 was markedly less active. The yields of ETBE at maximum IB conversion obtained over a dealuminated large-port mordenite and Omega (LZ-6) were 8 and 5%, thus in the range of values found for the US-Y and ZSM-5, respectively.

The yields versus temperature curves obtained over the commercial Beta zeolites and the reference Amberlyst-15 are compared in Fig. 3. B25*, B75, and Bsc, with nearly identical acid content (Table 1), exhibited similar catalytic performances and were less active than the resin, while B25, with more acid sites, was a little more active than the resin (yield of 27% at 54°C vs 25% at 60°C). Greater amounts

TABLE 3

Yield of ETBE at 45°C, at Maximum IB to ETBE Conversion (Ymax, mol %), Temperature at Maximum Conversion (Tmax, °C), and Yield of Di-isobutenes at 100 C (YC8, mol %)

	Y45	Ymax	Tmax	YC8
Amb.-15	5	25	60	7
H-Beta				
Bsc	4	20	65	8
B75	3	19	65	11
B25	15	27	55	14
B25*	3	20	67	3
B25* 0.02	5	22	64	11
B25* 0.03	7	23	60	12
B25* 0.05	4	22	60	12
B25* 0.06	6	21	66	9
B25* 0.09	3	20	66	13
lB18t c	23	28	53	15
lB18t cec	22	29	55	14
lB28t c	30	31	48	21
lB28t cec	28	31	51	15
lB36t c	15	28	55	13
lB36t cec	23	30	55	14
B25t c	21	32	51	19
B25t cec	23	33	46	19
B25t 0.1 c	32	34	50	18
US-Y				
CBV500	0	8	86	0
CBV600	0	9	80	1
CBV712	0	10	80	0
CBV760	0	11	80	1
CBV780	0	9	86	0
H-ZSM-5				
CBV3020	0	5	92	1
CBV5020	0	5	95	0
CBV8020	0	5	95	0
CBV2802	0	3	105	0
H-Mordenite				
M-S600H6	0	8	80	2
H-Omega				
LZ-6	0	5	90	0

of ETBE were produced over B25t c, B25t cec, and B25t 0.1-c with, at maximum IB to ETBE conversion, yields between 32 and 35% (25% for the resin), namely, a relative increase of between 28 and 40%. These three samples exhibited high conversions below 40°C. It has to be remarked that the comparison with the resin may be questionable since this catalyst is normally used in liquid phase conditions where the polar medium causes a swelling of its microreticular structure, which may substantially influence the catalytic performance. However, B25 was slightly more active at low temperatures than Amberlyst-15 (15) in vapor phase synthesis of MTBE; it was significantly more efficient than the resin in liquid phase conditions (20).

The results obtained over samples of B25* leached with nitric acid and calcined at 400°C are given in Table 3. Dealumination had a beneficial effect on the catalytic performances, except for the sample treated with 0.09 M nitric acid, which also contained less acid sites. A treatment with 0.02–0.05 M solutions (Si/Al ratio in the range 17.4–22) gave the best results, but the yields of ETBE at maximum conversion remained below that of the resin. This table also shows that the lab-synthesized samples that were either calcined (samples lBt c) or calcined, ammonium-exchanged, and decationed (samples lBt cec) were all more active than the other H-Beta zeolites and Amberlyst-15, with yields of ETBE at maximum conversion above 28%. None of these samples, however, equalized the performance of B25t 0.1 c, the most efficient sample (Fig. 3).

For all the Beta zeolites, the selectivity to ETBE was 100% in the temperature range 36–55°C (up to the maximum yield of ETBE). Di-isobutenes started to appear at temperatures beyond that of maximum IB to ETBE conversion and, at 100°C, substantial amounts were produced over the most active samples. The other common side reaction products in the synthesis of ETBE (43), namely, *tert*-butyl alcohol, diethyl ether, and 2,4,4-trimethyl-2-ethoxypentane, were also identified in the reaction products, but in amounts less than 1%.

DISCUSSION

The activity of the different zeolites followed the sequence: H-Beta > US-Y ≥ H-mordenite > ZSM-5 = Omega. It has been shown in the synthesis of MTBE that the catalytic performance could not be related to a single characteristic feature of the zeolite, but merely to the resultant of several factors acting together, with some having a prevailing influence (15). Since the reaction mainly occurs at the periphery of the zeolite crystallites, it is expected that the Beta zeolites, with higher external surface area (S_{ext}), will be more active than those with lower S_{ext}. Another feature distinguishing Beta zeolites from the other zeolites is the higher hydroxyl contents of the former ones, which intervene as adsorption sites for the alcohol molecules (16–19, 31, 33, 34). These aspects will be briefly discussed hereafter.

As shown in Fig. 4, the yield at maximum IB to ETBE conversion is proportional to the external surface area (S_{ext}) of the zeolite. It verifies similar relationships obtained in previous studies (15, 20) where it was inferred that the reaction was strongly diffusion limited. The external surface area was also an important parameter in the alkylation of isobutane with 1-butene (44) and in that of phenol with *tert*-butyl alcohol (45). However, the sole external surface area cannot account for the differences of activity observed among the H-Beta zeolites. Indeed, although the series of H-Beta zeolites had similar S_{ext}, the lab-synthesized samples (lBt) and those derived from B25t (with template) were substantially more active than B25, B25* (and the acid-leached forms), B75, and Bsc (Fig. 4 and Table 3), therefore pointing to the intervention of other factors.

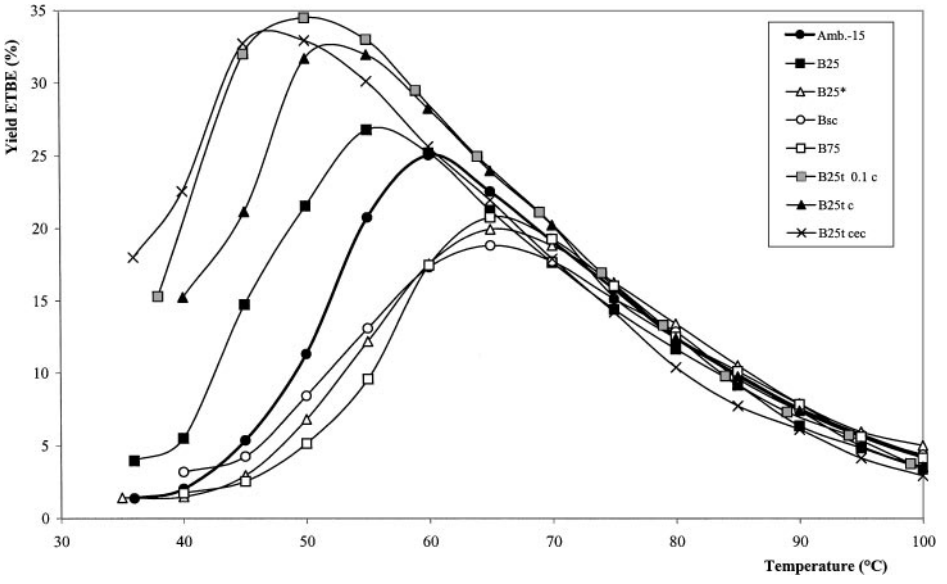

FIG. 3. Variation of the yield of ETBE vs reaction temperature over commercial Beta zeolites and Amberlyst-15.

Partial dealumination (increasing Si/Al ratio) enhanced the ETBE yield by increasing the accessibility of the acid sites (e.g., US-Y zeolites) and/or removing some EFAL species (e.g., the acid-leached forms of B25*). For the Beta zeolites, the yield at 45°C (and at maximum conversion) increased with the total amount of acid sites determined by NH_3-TPD, as shown in Fig. 5. The different slopes are interpreted as an indication that at low temperature (and conversion), the reaction occurs at the external surface and partly in the micropores of the zeolite. At maximum IB to ETBE conversion (higher temperatures), the less marked acidity effect suggests that the reaction is more diffusion limited and merely takes place at the external surface.

It has been observed in the vapor phase synthesis of MTBE that the presence of EFAl species had a negative effect on the reaction (15). This effect was clearly established for the series of US-Y zeolites for which a linear relationship exists between the reaction rate at 60°C and the proportion of EFAL species quantified by ^{27}Al MAS NMR spectroscopy (signals at 0 and 30 ppm) (29). CBV760, with the lowest EFAL content, was the most active one. In the present study, this zeolite is also more active among the series of US-Y zeolites. The higher yields of ETBE obtained over B25 relative to B25* can be accounted for by the same reason. These two zeolites have, indeed, similar Si/Al ratios but different amounts of acid sites, as found by

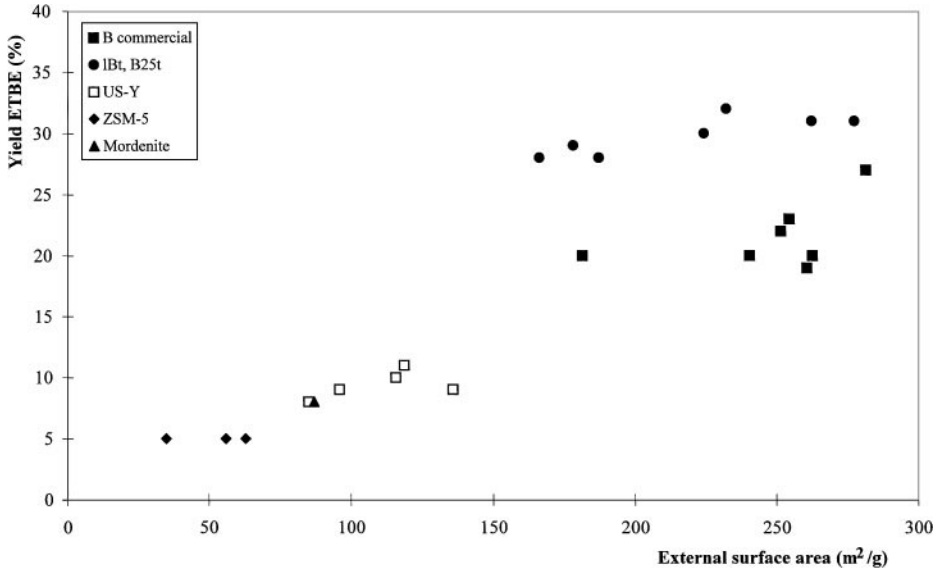

FIG. 4. Yield at maximum IB to ETBE conversion vs external surface area of the different zeolites.

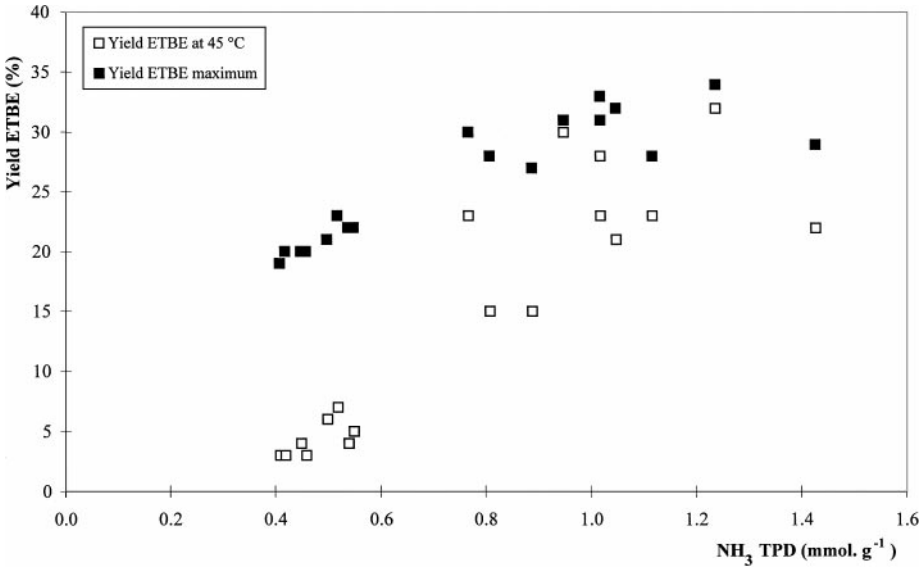

FIG. 5. Beta zeolites: yield of ETBE at 45°C and maximum conversion vs acid content measured by NH_3-TPD.

NH_3-TPD (Table 1) as well as by the normalized area of the AlOHSi band at 3610 cm^{-1} (Table 2), both pointing to the presence of EFAL species in B25*. Quantitative ^{27}Al MAS-NMR analysis of sample B25* showed the presence of 58% Al^{IV} (signal at 54 ppm), 25% Al^{VI} (0 ppm), the difference (17%) obtained by subtracting the Al content established by quantitative ^{27}Al MAS-NMR from that determined by ICPS representing the "invisible" Al. Removal of these EFAL species by mild acid leaching had a beneficial effect on the catalytic performances.

The zeolites lBt and B25t exhibited higher acid contents and bridging AlOHSi than the other Beta zeolites investigated (Fig. 1 and Table 2). Figure 6 shows the relationship between the yields of ETBE at 45°C and the amount of acid sites. Similar yields were reached for samples having high contents of AlOHSi sites (lBt). These samples were also characterized by the presence of fewer silanol groups at the outer surface of the crystallites (band at 3743–45 cm^{-1}). Hunger and co-workers (16–19) proposed that the SiOH groups act as a reservoir of reactant, forming clusters of alcohol molecules near the active sites. Plotting the ETBE yields against the SiOH/AlOHSi normalized band area ratio of different Beta zeolites (Fig. 7) shows that those with large ratios are less active and,

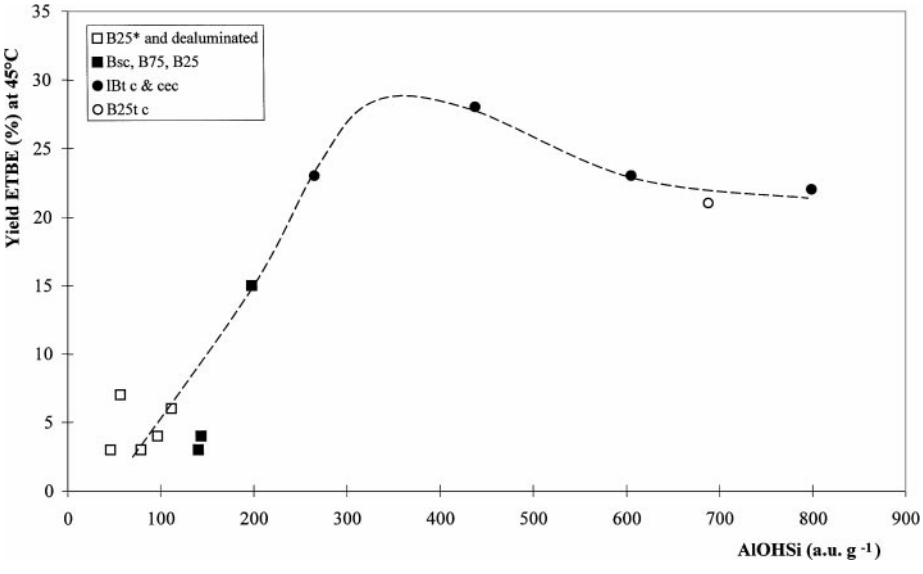

FIG. 6. Beta zeolites: yield of ETBE at 45°C and maximum conversion vs normalized band area of bridging AlOHSi groups (a.u. g^{-1}).

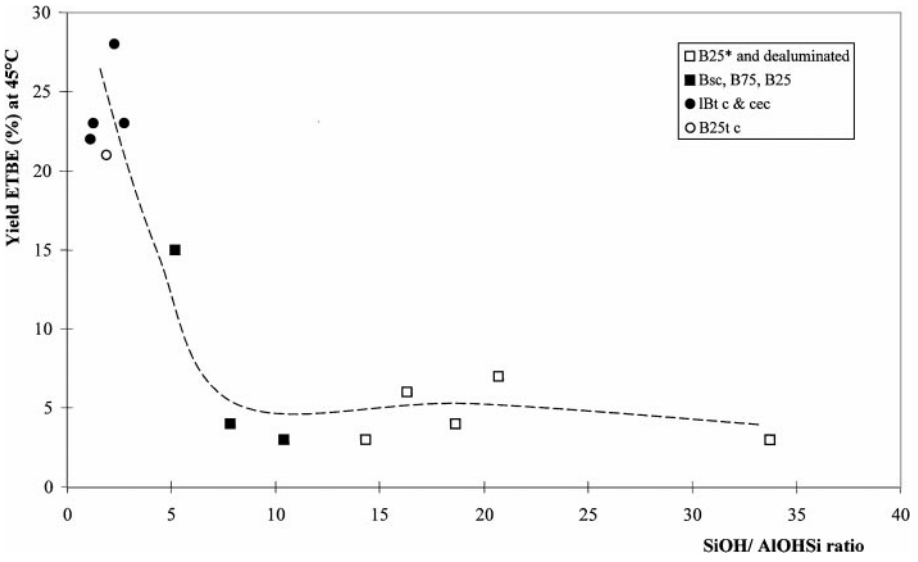

FIG. 7. Beta zeolites: yield of ETBE at 45°C and maximum conversion vs SiOH/AlOHSi normalized band area ratio.

conversely, the more active ones have smaller ratios, with the most active catalysts apparently describing an optimal SiOH/AlOHSi value. This suggests that ETBE synthesis over Beta zeolites is favored by a high amount of bridging AlOHSi (active sites) and a moderate amount of SiOH groups at the external surface, preventing the formation of too large and/or numerous ethanol clusters inhibiting the access of isobutene to the AlOHSi acid sites.

No significant effect on the yield of ETBE was noticed whether calcination of Beta zeolites to remove the template was followed by an ammonium-exchange or not (compare lBt cec and lBt c, and B25t cec and B25t c, Table 3). It has been reported that for an Al/(Al + Si) molar ratio of 0.085 (Si/Al = 10.8), all the template molecules are associated with framework Al, with the Na cations being located at structural defects (SiONa) (46). However, it has been shown that the ammonium ions resulting from the decomposition of the template (tetraethyl ammonium) occupy negative $SiOAlO_3Si_3$ centers, with the protons generated by decationation neutralizing the negatively charged framework sites (47). These observations may explain the catalytic results. For these samples, the similar amounts of acid sites determined by NH_3-TPD (Table 1), on the one hand, and the corresponding yields of ETBE (Table 3), on the other hand, are therefore consistent.

Obviously, the activity was improved when Beta zeolite still containing its template (B25t) was treated with 0.1 M nitric acid prior to the thermal decomposition of the template (B25t 0.1 c). This particular sample produced 32% ETBE at 45°C, a substantial gain compared with the other Beta samples and the acid resin, thus pointing to the beneficial effect using this activation method.

CONCLUSION

Vapor phase synthesis of ETBE performed over different acid zeolites has shown the following sequence of activity: Beta zeolite > US-Y > Mordenite > Omega ≥ ZSM-5. Beta zeolites, with external surface area above 200 $m^2\,g^{-1}$, are much more active than the other zeolites. At maximum isobutene to ETBE conversion, the lab-synthesized Beta zeolites produce more ETBE than the commercial samples and acid resin. Both Beta zeolites and Amberlyst-15 are 100% selective below 55°C. The reaction occurs on bridging AlOHSi acid sites of the zeolites, with higher yields of ETBE for those with high content of acid sites (AlOHSi) and low SiOH/AlOHSi ratios, where the number of ethanol clusters around the silanol groups still allows an easy access of isobutene to the AlOHSi active sites. Extra-framework Al species have a detrimental influence on the reaction, and their removal by a mild acid leaching is beneficial. Calcination of as-synthesized Beta zeolites to remove the template without and with subsequent ammonium exchange and thermal decomposition provide or a treatment with diluted acid prior to the elimination of the template provide very efficient catalysts.

ACKNOWLEDGMENTS

F. Collignon gratefully acknowledges F. R. I. A. (Fonds pour la Formation à la Recherche dans l'Industrie et l'Agriculture), Belgium, for a doctoral grant. The authors are indebted to P. Grobet, (Centrum voor Oppervlaktechemie en Katalyse, K. U. Leuven), for the ^{27}Al MAS-NMR measurements.

REFERENCES

1. Hälsig, C. P., Gregory, P., and Peacock, T., *Spec. Publ.—R. Soc. Chem.* **97**, 311 (1991).

2. Peaff, G., *Chem. Eng. News* 8, Sept. 26 (1994).
3. Karinen, R. S., and Krause, A. O. I., *Catal. Lett.* **67**, 73 (2000).
4. Leprince, P., and Travers, P., *in* "Le raffinage du pétrole. 3 Procédés de transformation," p. 299. Publ. IFP, Technip, Paris, 1998.
5. Vicencio, G. T., Ramos, A. O., Villanueva, J. R., and Lopez, G. P., *Rev. Inst. Mexicano Petrol.* **24**, 63 (1992).
6. Françoisse, O., and Thyrion, F. C., *Chem. Eng. Process.* **30**, 141 (1991).
7. Sola, L., Pericas, M. A., Cunill, F., and Tejero, J., *Ind. Eng. Chem. Res.* **34**, 3718 (1995).
8. Fité, C., Iborra, M., Tejero, J., Izquierdo, J. F., and Cunill, F., *Ind. Eng. Chem. Res.* **33**, 581 (1994).
9. Cunill, F., Vila, M., Izquierdo, J. F., Iborra, M., and Tejero, J., *Ind. Eng. Chem. Res.* **32**, 564 (1993).
10. Izquierdo, J. F., Cunill, F., Vila, M., Iborra, M., and Tejero, J., *Ind. Eng. Chem. Res.* **33**, 2830 (1994).
11. Tau, L.-M., and Davis, H., *Appl. Catal.* **53**, 263 (1989).
12. Larsen, G., Lotero, E., Marquez, M., and Silva, H., *J. Catal.* **157**, 645 (1995).
13. Fricke, R., Richter, M., Zubowa, H. L., and Schreier, E., *in* "Studies in Surface Science and Catalysis," Vol. 105, p. 655. Elsevier Sci., Amsterdam, 1997.
14. Richter, M., Zubowa, H. L., Heckelt, R., and Fricke, R., *Microporous Mater.* **7**, 119 (1997).
15. Collignon, F., Mariani, M., Moreno, S., Remy, M., and Poncelet, G., *J. Catal.* **166**, 53 (1997).
16. Hunger, M., Horvath, T., and Weitkamp, J., *in* Proc. DGMK Conf. "C4 Chemistry-Manufacture and Uses of C4 Hydrocabons," p. 65. German Soc. Petrol. Coal Sci. Techn., 1997.
17. Hunger, M., and Horvath, T., *Catal. Lett.* **49**, 95 (1997).
18. Hunger, M., Horvath., T., and Weitkamp, J., *Microporous. Mater.* **22**, 357 (1998).
19. Horvath, T., Seiler, M., and Hunger, M., *Appl. Catal., A.* **193**, 227 (2000).
20. Collignon, F., Loenders, R., Martens, J. A., Jacobs, P. A., and Poncelet, G., *J. Catal.* **182**, 302 (1999).
21. Moreno, S., and Poncelet, G., *Microporous Mater.* **12**, 197 (1997).
22. Fajula, F., Bourgeat-Lami, E., Zivkov, C., Des Courières, T., and Anglerot, D., Fr. Patent. 2, 069, 618 (1992).
23. Borade, R. B., and Clearfield, A., *Microporous Mater.* **5**, 289 (1996).
24. Volosch, M., Ladisch, M. R., and Tsao, G. T., *React. Polym.* **4**, 9 (1986).
25. de Boer, J. H., Linsen, B. G., and Osinga, T. J., *J. Catal.* **4**, 643 (1964).
26. Niwa, M., Katada, N., Sawa, M., and Murikami, Y., *J. Phys. Chem.* **99**, 8812 (1995).
27. Katada, N., Iijima, S., Iigi, H., and Niwa, M., *in* "Studies in Surface Science and Catalysis," Vol. 105, p. 1227. Elsevier Sci., Amsterdam, 1997.
28. Coutanceau, C., Da Silva, J. M., Alvarez, M. F., Ribero, F. R., and Guisnet, M., *J. Chim. Phys.* **94**, 765 (1997).
29. Remy, M. J., Stanica, D., Poncelet, G., Feijen, E. J. P., Grobet, P. J., Martens, J. A., and Jacobs, P. A., *J. Phys. Chem.* **100**, 12440 (1996).
30. Bourgeat-Lami, E., Massiani, P., Di Renzo, F., Fajula, F., and Des Courières, T., *Catal. Lett.* **5**, 265 (1990).
31. Kiricsi, I., Flego, C., Pazzuconi, G., Parker, W. O., Jr., Millini, R., Perego, C., and Bellussi, G., *J. Phys. Chem.* **98**, 4627 (1994).
32. Beck, L. W., and Haw, J. F., *J. Phys. Chem.* **99**, 1076 (1996).
33. Jia, C., Massiani, P., and Barthomeuf, D., *J. Chem. Soc., Faraday Trans.* **89**, 3659 (1993).
34. Maache, M., Janin, A., Lavalley, J. C., Joly, J.-F., and Benazzi, E., *Zeolites* **13**, 419 (1993).
35. Guisnet, M., Ayrault, P., Coutanceau, C., Fernanda Alvarez, M., and Datka, J., *J. Chem. Soc. Faraday Trans.* **93**, 1661 (1997).
36. Pazé, C., Bordiga, S., Lamberti, C., Salvalaggio, M., Zecchina, A., and Bellussi, G., *J. Phys. Chem.* **101**, 4740 (1997).
37. Newsam, J., Treacy, M., Koetsier, W., and de Gruyter, C., *Proc. R. Soc. London, Ser. A* **420**, 375 (1988).
38. Treacy, M., and Newsam, J., *Nature* **332**, 249 (1988).
39. Vimont, A., Thibault-Starzyk, F., and Lavalley, J. C., *J. Phys. Chem. B* **104**, 286 (2000).
40. Su, B.-L., and Norberg, V., *Zeolites* **19**, 65 (1997).
41. Loeffler, R. E., Lohse, U., Peuker, Ch., Oelhmann, G., Kustov, L. M., Zholobenko, V. L., and Kazansky, V. B., *Zeolites* **10**, 266 (1990).
42. Emeis, A., *J. Catal.* **141**, 347 (1993).
43. Richter, M., Fisher, H., Bartoszek, M., Zubowa, H. L., and Fricke, R., *Microporous Mater.* **8**, 69 (1997).
44. Loenders, R., Martens, J. A., and Jacobs, P. A., *J. Catal.* **176**, 545 (1998).
45. Zhang, K., Huang, C., Zhang, H., Liu, S., Xu, D., and Li, H., *Appl. Catal., A* **166**, 89 (1998).
46. Vaudry, F., Di Renzo, F., Fajula, F., and Schulz, P., *in* "Studies in Surface Science and Catalysis," Vol. 84, p. 163. Elsevier Sci., Amsterdam, 1994.
47. Bougeat-Lami, E., Di Renzo, F., and Fajula, F., *J. Phys. Chem.* **96**, 3087 (1992).